Optimal Control of Methane Conversion to Ethylene

A. Faliks,[†] R. A. Yetter,[‡] C. A. Floudas,[§] R. Hall,[⊥] and H. Rabitz*,[†]

Departments of Chemistry, Mechanical and Aerospace Engineering, and Chemical Engineering, Princeton University, Princeton, New Jersey 08544, and Exxon Research and Engineering, Annandale, New Jersey 08801

Received: May 16, 2000

An optimal control methodology is applied to the problem of finding the heat, hydrogen, and oxygen flux profiles for the homogeneous gas-phase conversion of methane to ethylene in a plug flow reactor. The calculations use a detailed reaction model for the oxidative pyrolysis of methane and a model for the growth of polycyclic aromatic hydrocarbons and soot particle nulceation and growth. The reactor designs show that distributed hydrogen and oxygen fluxes along the axis of the reactor improve ethylene yields to a greater extent than co-fed hydrogen and/or oxygen. The axial heat flux is shown to play a major role in the final yields of ethylene. The optimal residence times are 28−31 ms, and the optimal temperature profiles cover a range of 1200−1985 K. The simulation results show that for the conditions considered, C_2H_2 is formed initially and is converted to C_2H_4 by a controlled extraction of energy. Hydrogen addition is advantageous at both stages to reduce soot in the first half of the reactor and to shift the equilibrium toward ethylene in the second half. Oxygen aids in forming ethylene from the C_2H_5 and C_2H_3 intermediates and in the formation of hydrogen radicals. Ethylene carbon mass fractions of 0.64 have been achieved. The solutions, although not proven to be globally optimal, are of high quality.

1. Introduction

Recent efforts to locate new petroleum reserves have increasingly found new hydrocarbons to be in the form of natural gas rather than crude oil. Consequently, much research has been focused on developing processes for the conversion of natural gas to liquid fuels and other chemicals. Several approaches have been studied. For example, it has been widely demonstrated that C_{2+} formation rates and selectivity may be increased by varying the CH_4/O_2 feed ratios in oxidative coupling. To maintain a low oxygen concentration at a local point within the reactor, equally distributed feeds of O_2 along the length of the reactor have been suggested and studied theoretically (Santamaria et al., 1991, 1992;[1] Reyes et al., 1993[2,3]) and experimentally (Choudhary et al., 1989[4]; Smith et al., 1991.[5]) The work of Reyes et al., in particular, presents a detailed reaction transport model where up to 200 discrete oxygen injection points are considered. The theoretical yields obtained are as high as 50%. Comparably high experimental yields have also been obtained in the work of Olsvik et al.[6] who examined CH_4/H_2 co-feeds in homogeneous hydropyrolysis of methane.

However, none of the above efforts have attempted to optimize the distribution of energy and/or mass along the reactor length. The chemical yields from any particular reactor design represent a lower bound on what might be achieved. Thus, it is desirable to explore the improved product yields from an optimal design of distributed energy and input chemical flux along the length of the reactor.

Rojnuckarin et al.[7] utilized an optimal control approach to find flux profiles that maximize the conversion of methane to ethylene in a plug flow reactor. The mechanism used in their work did not incorporate the formation of soot. High yields of ethylene were achieved with distributed heat and oxygen fluxes. In this paper, hydrogen fluxes will be examined in addition to heat and oxygen fluxes. The application of the algorithm to a plug flow reactor is very similar to that described by Faliks et al.[8] where high-quality solutions were obtained for the conversion of methane to acetylene. In this work, optimization is carried out with a detailed reaction mechanism of 81 species and 443 reactions and a model for the growth of polycyclic aromatic hydrocarbons (PAH's) and soot particle nucleation and growth, developed by Frenklach and Wang.[9] In addition, the current work investigates distributed injection of hydrogen and oxygen.

In section 2, the reactor model is presented. In section 3, several optimal control designs are shown and important mechanistic steps are discussed. Finally, section 4 presents conclusions that consider the applicability of the process and its laboratory implementation.

2. Modeling

2.1. Physical Formulation of the Flow Reactor. A plug flow reactor (PFR) was chosen as the basic reactor configuration. The PFR was a cylinder with constant cross sectional area and length L. Control is implemented through chemical and/or heat flux through the side wall of the reactor as a function of the position l along its length. The reactions are described by the production rate w_i of the ith species, $i = 1, ..., n$. The control variables are the fluxes of species i, denoted as j_i (mass/length − time), and the heat flux, q (energy/length − time), as a function of position l. The mass fraction of species i in the reactor is denoted as $x_i(l)$, and the total mass flow rate is $F(l)$.

The following assumptions were made in modeling the PFR: (i) steady one-dimensional plug flow, (ii) instantaneous radial mixing, (iii) no diffusion along the axis of the reactor, and (iv) adiabatic reaction conditions. To make the assumptions

[†] Deparment of Chemistry, Princeton University.
[‡] Deparment of Mechanical and Aerospace Engineering, Princeton University.
[§] Deparment of Chemical Engineering, Princeton University.
[⊥] Exxon Research and Engineering.

10.1021/jp001797j CCC: $19.00
Published on Web 11/01/2000

realistic, the ratio of the length of the reactor to its radius was chosen to be greater than 25.

Since there are two sources of material flowing into the system (however, the co-feed input is coincident with $j(0)$), the total mass balance for the flow rate is

$$F(l) = F(0) + \int_0^l \sum_{i=1}^{n} j_i \, \mathrm{d}l$$

where j_i is the ith component of the vector j and n is the number of components in the mixture.

By taking a differential control volume at position l and balancing the input and output mass and energy, we can arrive at the equations governing the composition in the reactor. Considering the conservation of mass, the species balance equation is

$$Fx_i + j_i \, \mathrm{d}l + w_i \, \mathrm{d}l = \left(F + \frac{\mathrm{d}F}{\mathrm{d}l}\mathrm{d}l\right)\left(x_i + \frac{\mathrm{d}x_i}{\mathrm{d}l}\mathrm{d}l\right)$$
$$= (F + \sum_{i=1}^{n} j_i \, \mathrm{d}l)\left(x_i + \frac{\mathrm{d}x_i}{\mathrm{d}l}\mathrm{d}l\right)$$

The first term on the left represents the amount of the ith species flowing into the control volume. The second and third terms, respectively, represent the amount of the species in influx added from the side of the reactor and the amount produced or consumed in chemical reactions within the volume. Taking the infinitesimal limits of $\mathrm{d}x_i$ and $\mathrm{d}l$, we arrive at the mass conservation equation:

$$\frac{\mathrm{d}x_i}{\mathrm{d}l} = \frac{1}{F}(w_i - x_i \sum_{k=1}^{n} j_k + j_i)$$

A similar approach is used to derive the energy conservation equation:

$$T\sum_{i=1}^{n} C_{pi}Fx_i + (T_0 \sum_{i=1}^{n} C_{pi}j_i + q) \, \mathrm{d}l - \sum_{i=1}^{n} H_{fi}w_i \, \mathrm{d}l$$
$$= (T + \mathrm{d}T)\left[\sum_{i=1}^{n}\left(F + \frac{\mathrm{d}F}{\mathrm{d}l}\mathrm{d}l\right)\left(x_i + \frac{\mathrm{d}x_i}{\mathrm{d}l}\mathrm{d}l\right)C_{pi}\right]$$
$$= \left(T + \frac{\mathrm{d}T}{\mathrm{d}l}\mathrm{d}l\right)\left[\sum_{i=1}^{n}(F + \sum_{i=1}^{n} j_i \, \mathrm{d}l)\left\{x_i + \left(\frac{1}{F}(w_i - x_i\sum_{k=1}^{n} j_k + j_i)\right)\mathrm{d}l\right\}C_{pi}\right]$$

where q is the heat influx, H_{fi} is the heat of formation of species i, and C_{pi} is the corresponding specific heat. T_0 is the temperature of the influxed species. Taking the infinitesimal limits of $\mathrm{d}x_i$ and $\mathrm{d}l$ leads to the energy conservation equation:

$$\frac{\mathrm{d}T}{\mathrm{d}l} = \frac{1}{F\sum C_{pi}x_i}((T_0 - T)\sum_{i=1}^{n} C_{pi}j_i - \sum_{i=1}^{n} H_{fi}w_i - T\sum_{i=1}^{n} C_{pi}w_i + q)$$

In the calculations, the CONMIN[10] code was used as the conjugate gradient minimizer; the chemical kinetics package CHEMKIN-II[11] was employed to interface the thermodynamic and kinetics data; LSODA[12] was used as a differential equation integrator, and AIM[13] was used in the sensitivity analysis.

2.2. Chemical Model. The chemical model used in this paper has two parts. The first is a detailed reaction mechanism of 81 species and 443 reactions developed by Frenklach and Wang.[9] This mechanism describes methane pyrolysis and oxidation. It includes pathways for the production of acetylene and other C_2 hydrocarbons, as well as higher order molecules such as benzene. The mechanism also allows for oxidation of acetylene to CO or CO_2 and polymerization of acetylene to form higher order hydrocarbons.

The second part of the model describes poly(PAH) and soot formation. The PAH and soot formation model consists of four major processes: initial PAH formation; replicating-type growth of PAH; particle nucleation, consisting of coalescence of PAH into three-dimensional clusters; and particle growth by coagulation and surface reactions of the forming clusters and particles.[8]

At high temperatures, the formation of the first aromatic ring begins with vinyl addition to acetlyene to form vinylacetylene. This is followed by acetylene addition to the n-C_4H_3 radical formed by H atom abstraction from the vinylacetylene.

The minimal reaction set that describes PAH growth is given as:

$$\mathrm{A}_i + \mathrm{H} = \mathrm{A}_{i-} + \mathrm{H}_2$$

$$\mathrm{A}_{i-} + \mathrm{C}_2\mathrm{H}_2 = \mathrm{A}_i\mathrm{C}_2\mathrm{H}_{2-}$$

$$\mathrm{A}_i\mathrm{C}_2\mathrm{H}_{2-} + \mathrm{C}_2\mathrm{H}_2 = \mathrm{A}_{i+1} + \mathrm{H}$$

where A_i is the aromatic molecule containing i fused aromatic rings, and A_{i-} is an aromatic radical formed by the abstraction of an H atom from A_i. It is assumed the first two reactions are reversible while the third is not.

PAH and particle growth is modeled by the technique of linear lumping. In this method, a small number of differential equations developed for the moments of the PAH and particle distribution functions describe the kinetics of an infinite sequence of polymerization-type reactions of PAH and particle growth.[14,15]

The moments are defined in two ways. First are the concentration moments, given by

$$M_r^{\mathrm{PAH}} = \sum_{i=i_0}^{\infty} m_i^r \, N_i^{\mathrm{PAH}}$$

where M_r^{PAH} is the rth concentration moment of the distribution of the PAH species concentration, i_0 is the initial PAH size from which the lumping begins and the summation is over all PAH species above this size, and m_i and N_i^{PAH} are the mass and number concentration, respectively, of the PAH species of size class i. The PAH mass is represented by the number of carbon atoms.

The second type of moments are the size moments:

$$\mu_{\mathrm{r}}^{\mathrm{PAH}} = \frac{M_r^{\mathrm{PAH}}}{M_0^{\mathrm{PAH}}}$$

The concentration moment M_1^{PAH} gives the total PAH mass (i.e., the total number of carbon atoms accumulated in PAH species per unit volume). The size moment μ_1^{PAH} gives the average PAH size (i.e., the average number of carbon atoms per PAH).

The equations for the concentration moments are

$$\frac{dM_0^{PAH}}{dt} = r_0$$

$$\frac{dM_1^{PAH}}{dt} = m_0 r_0 + \sum_{l=1}^{l_c} \Delta m_l R_l^{[0]}$$

$$\frac{dM_2^{PAH}}{dt} = m_0^2 r_0 + \sum_{l=1}^{l_c} \Delta^{[2]} m_l R_l^{[0]} + 2\Delta_c m \sum_{l=1}^{l_c} \Delta m_l R_l^{[1]}$$

...

$$\frac{dM_r^{PAH}}{dt} = m_0^r r_0 + \sum_{j=0}^{r-1} \binom{r}{j} (\Delta_c m)^j \sum_{l=1}^{l_c} \Delta^{[r-j]} m_l R_l^{[j]}$$

where

$$\Delta^{[p]} m_l = (m_l - \Delta_c m)^p - (m_{l-1} - \Delta_c m)^p, \quad l = 1, 2, ..., l_c$$

$$\Delta_c m = \sum_{l=1}^{l_c} \Delta m_l = \sum_{l=1}^{l_c} (m_l - m_{l-1}) = m_{i+l_c} - m_i$$

In these equations, r_0 is the rate of formation of the first lumped species, m_0 is the number of carbon atoms in the first lumped species, l is the number of mass-addition reactions of the replicating sequence (there are a total of l_c such reactions), m_l is the number of carbon atoms of the reactant PAH in the lth mass-addition reaction, $\Delta m_l = \Delta^{[0]} m_l$ is the number of carbon atoms added in the lth mass-addition reaction, $\Delta_c m$ is the number of carbon atoms added during the entire replicating cycle, and $R_l^{[j]}$ is the net flux of j-lumped reaction l. The rates of formation for lumped species and $R_l^{[j]}$ are given by Frenklach and Wang.[9]

The formation and evolution of soot particles was described by moments similar to the PAH moments:

$$M_r^{soot} = \sum_{i=i_0}^{\infty} m_i^r N_i^{soot}$$

$$\mu_r^{soot} = \frac{M_r^{soot}}{M_0^{soot}}$$

where M_r^{soot} and μ_r^{soot} are the rth concentration and size moments, respectively, of the soot particle distribution; and m_i and N_i^{soot} are the mass and number density, respectively, of the soot particles of size class i. As in the PAH formulation, the soot particle mass was represented by the number of carbon atoms.

The concentration moments are described by the following equations:

$$\frac{dM_0^{soot}}{dt} = R_0 - G_0$$

$$\frac{dM_1^{soot}}{dt} = R_1 + W_1$$

$$\frac{dM_2^{soot}}{dt} = R_2 + G_2 + W_2$$

...

$$\frac{dM_r^{soot}}{dt} = R_r + G_r + W_r$$

where R, G, and W are the nucleation, coagulation, and surface rate terms, respectively.[8]

The nucleation term consists of the formation of soot particles initiated by coalescence of two PAH species into a dimer.[8] The coagulation terms G are defined previously.[15] The surface growth term W is due to the addition of mass by C_2H_2 and PAH and oxidation by O_2 and OH.[8,16]

3. Computational Studies

The optimal control design formulation was applied to several test problems. In each example, an effective strategy for finding a cost functional minimum involved making a few runs with increasingly demanding objectives. The optimal flux profiles of the previous run were found to be good initial points for subsequent runs. The computer code employed for these simulations has also been used-in previous applications[7,9] and has performed well. It is important to note that the present work serves to show the potential significance of optimally controlling methane pyrolysis to C_2 products rather than attempting to corroborate any specific reaction mechanism.

The average iteration took about 31 min of CPU time on an R4000 IRIS Indigo. Although global optimality could not be guaranteed, it is evident that good quality solutions were obtained using the proposed algorithm.

In all the examples, the length of the PFR in which the reactions proceed is $L = 100$ cm, with a cross-sectional area of 40 cm^2. The optimal inlet flow rate at $l = 0$ was determined by trial and error. The reactor is at a constant pressure of 1 atm. In the examples where oxygen was co-fed, the initial composition of the feedstock was chosen as 97% CH_4, 2% O_2, and 1% C_2H_6 by mass. Ethane was added to the methane to simulate the kinetic effects of small amounts of higher molecular weight hydrocarbons typically found in natural gas. In the examples where oxygen addition was distributed along the reactor length, the initial composition of the feedstock was chosen as 99% CH_4 and 1% C_2H_6 by mass. In considering the examples, the ethylene yield is expressed in terms of carbon mass fractions (carbon in ethylene divided by total carbon), and even a small change could eventually be significant at least for its indicated direction of change.

Example 1 uses a heat flux to achieve optimal ethylene yields. Example 2 uses a heat flux and a hydrogen flux to improve on the results of example 1. Example 3 attempts to improve on the results of example 2 by using a heat flux, a hydrogen flux, and an oxygen flux. Example 4 uses a heat flux but places a moving weight on the soot carbon mass fraction. Further studies could be considered, but these serve to illustrate some physical points and what might be achieved from such a distributed control reactor.

The optimal residence time was found by optimizing yields at several initial flow rates and choosing the initial flow rate that resulted in the highest yield.

3.1. Example 1: Heat Flux. Due to the importance of temperature to reaction rates, a natural question to pose is: What is the optimal distibution of energy flux along the reactor length that will maximize ethylene yields? Example 1 attempts to answer that question by optimizing the heat flux (and thus producing a beneficial temperature profile). The heat flux proved to be the most important variable for control purposes.

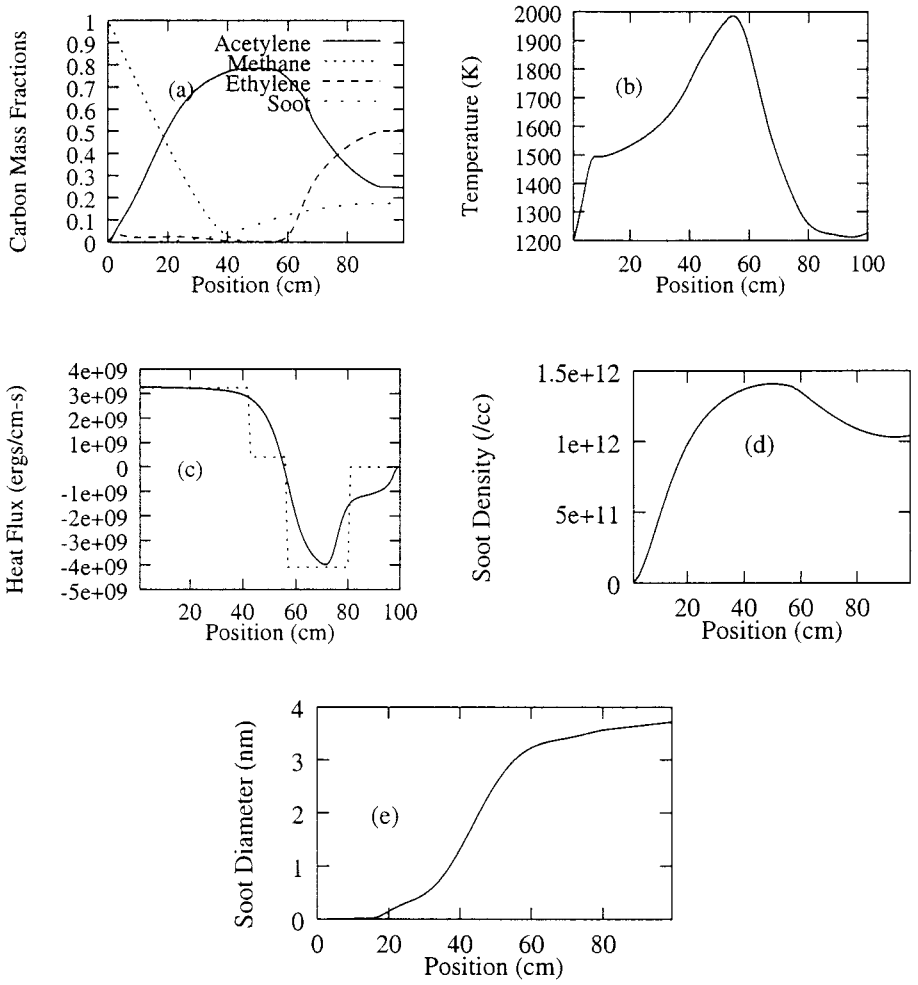

Figure 1. Results from example 1; optimization of heat flux (28.75 ms residence time): (a) Carbon mass fraction trajectories. (b) Temperature profile at optimal solution. (c) Optimal heat flux. The solid line corresponds to example 1. The dotted line corresponds to the optimized flux regions. (d) Soot particle number density. (e) Soot particle average diameter.

The results of example 1 are shown in Figure 1. The optimal residence time is 28.75 ms. The final ethylene carbon mass fraction is 0.51 and the soot carbon mass fraction is 0.18. The soot particle number density is 1.0×10^{12} cm^{-3} and the average soot particle diameter is 3.6 nm. The formation of soot becomes significant only when the temperatures reaches about 1500−1600 K. This is consistent with experimental evaluation of the critical temperatures of soot formation.[17]

For this example, the residence time was optimized to give maximum ethylene yield without regard to soot.

In order to demonstrate the flexibility of the model we considered a heat flux separated into regions instead of a continuous one. The length of the regions and the heat flux at each region were optimized. Figure 1c shows the optimized heat flux of four regions. The ethylene and soot yields, as well as the temperature profile, are identical to Example 1.

3.2. Example 2: Heat and Hydrogen Fluxes. Example 2 uses both a heat and a hydrogen flux to improve on the ethylene yields shown in example 1. The results are shown in Figure 2. The ethylene carbon mass fraction in this particular solution rises significantly to 0.63 and the soot carbon mass fraction drops to 0.15. The soot particle number density is 9.7×10^{11} cm^{-3} and the average soot particle diameter is 3.2 nm.

The solution shown in Figure 2 is a local solution for a residence time of 29.5 ms. Because of equilibrium considerations, the more hydrogen is added in the second half of the reactor, the higher the ethylene yield. It is possible to generate higher yields of ethylene by starting with an initial guess that provides a higher hydrogen flux in the second half of the reactor. As more hydrogen is added, the marginal improvement in ethylene yield becomes smaller. The hydrogen flux in the first half of the reactor, however, seems independent of the initial guess. This part of the hydrogen flux acts much like the hydrogen flux of the acetylene optimization runs carried out by Faliks et al.[8] It hinders soot formation by lowering the partial pressures and reducing the radical pool once acetylene is formed but before soot formation accelerates.

It is possible to place a weight on the heat flux in order to lower the temperature profile. A run with the same hydrogen flux as example 2 but with a moving weight on the heat designed to keep the temperature under 1750 K resulted in an ethylene carbon mass fraction of 0.57. The residence time was reduced to 27 ms.

3.3. Example 3: Heat, Hydrogen, and Oxygen Fluxes. In the first two examples, oxygen was co-fed into the system to aid in initiation. In this example, oxygen is allowed to enter the reactor as a distributed flux. The hydrogen flux and the residence time are the same as in example 2. This results in marginal improvements as shown in Figure 3. The ethylene carbon mass fraction rises to 0.635 while the soot carbon mass fraction remains at 0.15. The soot particle number density is 9.7×10^{11} cm^{-3} and the average soot particle diameter is 3.2 nm.

An oxygen co-feed mass fraction of 0.019 would represent the same amount of oxygen that was fluxed into the system in

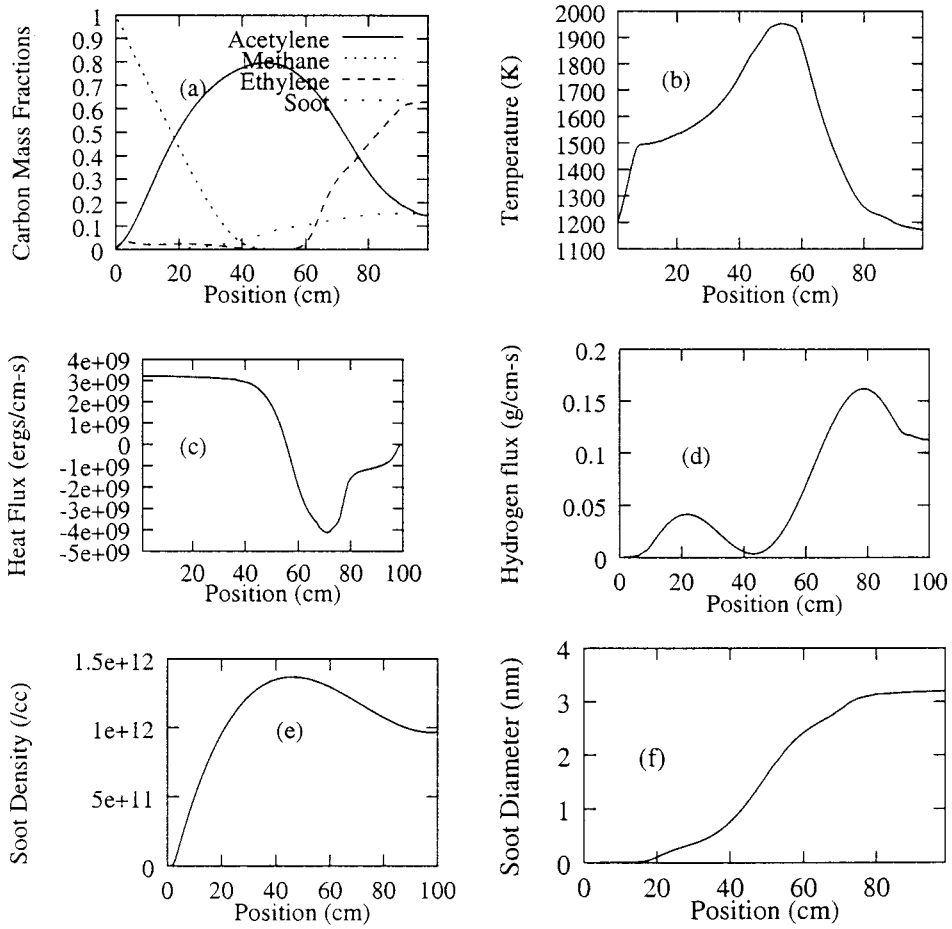

Figure 2. Results from example 2; optimization of heat and hydrogen fluxes (29.5 ms residence time): (a) carbon mass fraction trajectories; (b) temperature profile at local solution; (c) heat flux; (d) hydrogen flux; (e) soot particle number density; (f) soot particle average diameter.

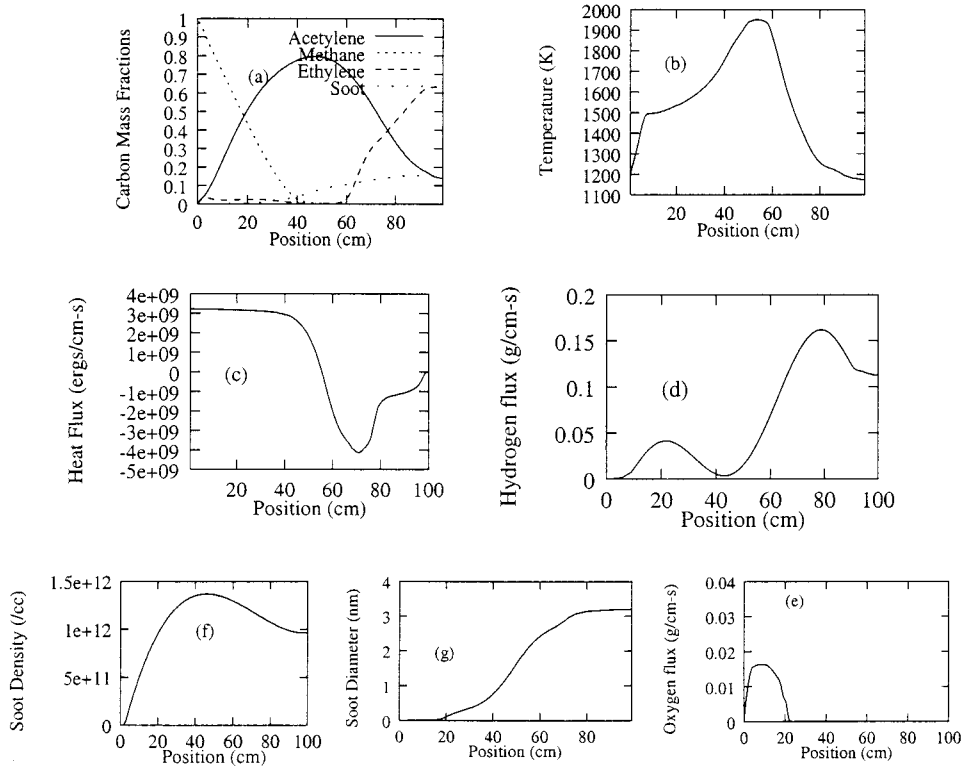

Figure 3. Results from example 3; optimization of heat, hydrogen, and oxygen fluxes (29.5 ms residence time): (a) carbon mass fraction trajectories; (b) temperature profile; (c) heat flux; (d) hydrogen flux; (e) oxygen flux; (f) soot particle number density; (g) soot particle average diameter.

example 3. A run with such an oxygen co-feed, however, shows no improvement over example 2. In addition, the optimal oxygen co-feed mass fraction is 0.022 but the resulting C_2H_4 carbon mass fraction is still 0.021% less than example 3. This

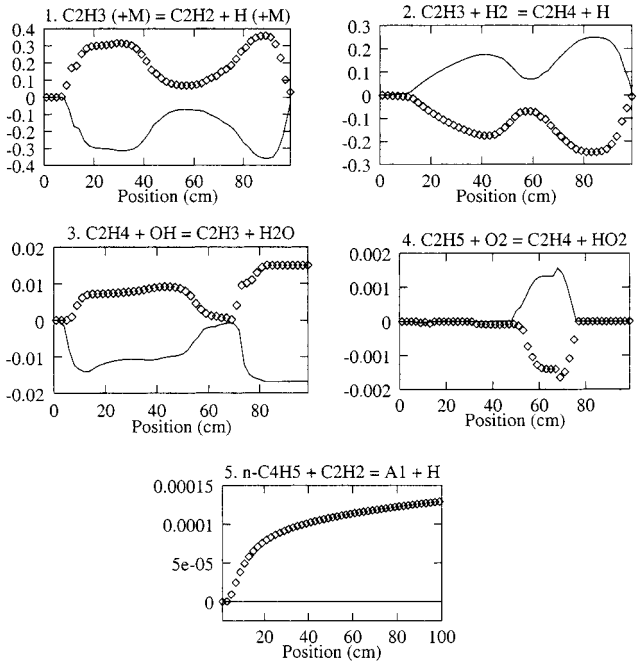

Figure 4. Normalized sensitivity coefficients of C_2H_4 mass fraction at the end of the reactor with respect to reaction rate constants $dx_{C_2H_4}/d\ln(k)$ for the five most sensitive reactions at the optimal solution of example 3. Solid lines correspond to the forward reaction, and diamond curves correspond to the reverse reaction.

shows that the distributed nature of the oxygen flux, not only its amount, is responsible for the improvements shown in example 3.

Figure 4 shows the results of the reaction sensitivity analysis. The five largest sensitivity coefficients of the C_2H_4 mass fraction with respect to each reaction rate constant $dx_{C_2H_4}/d\ln(k)$ are shown. The first two reactions demonstrate that the C_2H_4 is formed predominantly by H-atom addition to C_2H_2 to form C_2H_3 and eventually C_2H_4.

Further analysis is needed to investigate the benefits of a distributed oxygen flux. The reactions whose normalized sensitivity coefficients of C_2H_4 mass fraction at the end of the reactor with respect to reaction rate constants $dx_{C_2H_4}/d\ln(k)$ changed the most with a distributed oxygen flux versus co-fed oxygen are presented. The reactions are written so that the forward direction is the one that is beneficial for C_2H_4 creation (i.e., the forward reaction has a positive sensitivity):

$$OH + H_2 = H + H_2O \quad (1)$$

$$C_2H_3 + H_2O = C_2H_4 + OH \quad (2)$$

$$C_2H_5 + O_2 = C_2H_4 + HO_2 \quad (3)$$

$$C_2H_5 + O = CH_3 + CH_2O \quad (4)$$

Reactions 1 and 2 above provide an alternative route for C_2H_4 creation. In reaction 2, H_2O reacts with C_2H_3 to form C_2H_4 and OH. The OH then reacts with H_2 in reaction 1 to recycle H_2O and create H radicals which add to C_2H_3. This additional route may account for the marginal improvement in acetylene

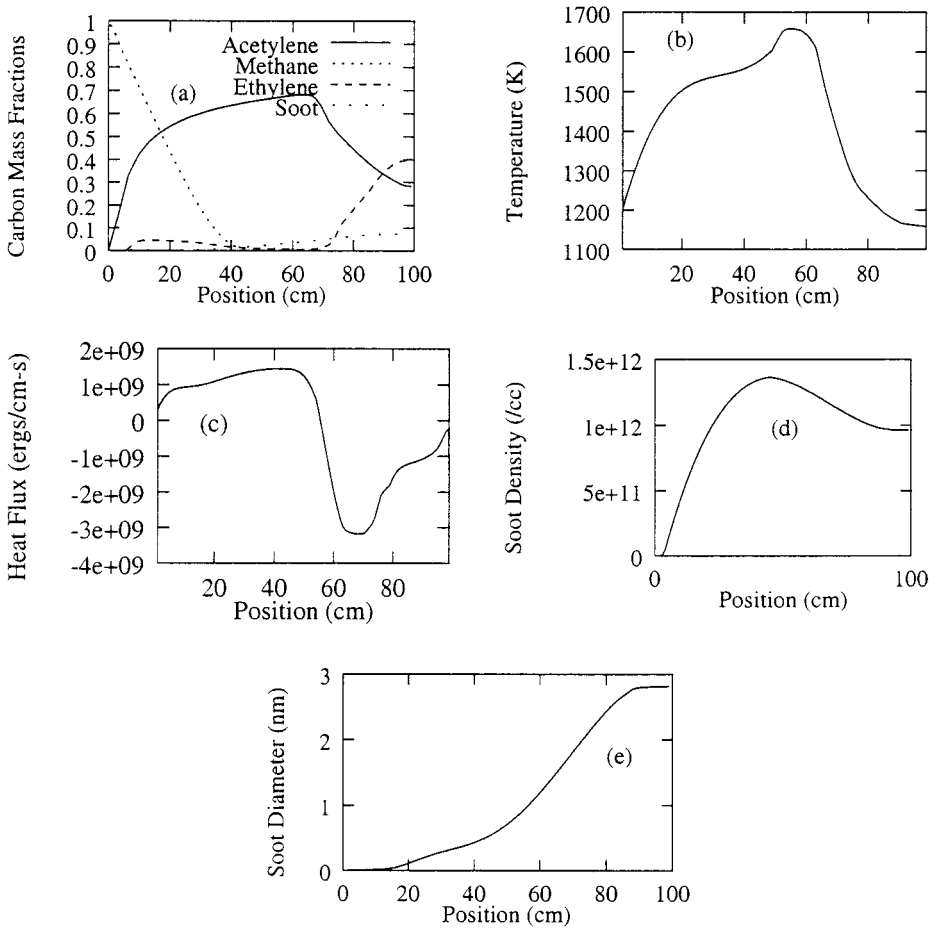

Figure 5. Results from example 4; optimization of heat flux with weight on soot formation (31 ms residence time): (a) carbon mass fraction trajectories; (b) temperature profile at optimal solution; (c) optimal heat flux; (d) soot particle number density; (e) soot particle average diameter.

conversion to ethylene. It should be noted that similar results are obtained if the oxygen flux is replaced with H_2O.

3.4. Example 4: Heat Flux With Weight on Soot Formation. To demonstrate that the optimal control approach is flexible enough to provide good yields under various conditions, we ran an optimization with a moving weight on the soot mass fraction. The goal was to optimize ethylene yields while keeping the soot carbon mass fraction under 0.10. The results are shown in Figure 5. The optimal residence time is 31 ms. The ethylene carbon mass fraction is 0.40 and the soot carbon mass fraction 0.076. The soot particle number density is 9.6×10^{11} cm^{-3} and the average soot particle diameter is 2.8 nm.

The temperature profile is reduced significantly so that very little of the residence time is spent at temperatures that are greater than 1500−1600 K, the temperature range shown to be critical for soot formation.[17] The lower temperature profile, however, reduces the production of acetylene and the conversion of acetylene to ethylene.

4. Conclusions

The optimal control of the conversion of methane to ethylene in a PFR has been considered in this paper. The chemical reaction model incorporated soot formation and revealed the inverse correlation between ethylene production and soot formation. It was shown that optimally designed heat, hydrogen, and oxygen fluxes along the length of the reactor are effective in minimizing soot and maximizing ethylene yields. Although hydrogen and oxygen co-feeds can increase ethylene yields, better results were obtained with distributed fluxes along the side of the reactor. The optimal residence times were found to be 28−31 ms. The temperature profiles covered a range of 1200−1985 K. Under various conditions, convergence to high-quality yields was achieved. In all cases, over 75% of the carbon mass was converted to useful C_{2+} hydrocarbons while soot formation was minimized. Since global optimality was not guaranteed, better results may be possible within the model. However, other non-modeled physical and chemical processes could alter the yields in either direction.

The increased yields that result from optimizing distributed fluxes show that enhancement of methane conversion to ethylene can be achieved by employing special reactor configurations. In the laboratory, the theoretical solutions presented in this paper can serve as starting points for a reactor with feedback control. The output performance of the reactor will be fed to a learning algorithm, to in turn design the next experiment in a repeated sequence. This self-optimization is independent of the model assumptions that were used in the theoretical work and will therefore bring, forth the most refined yields.

Acknowledgment. The authors acknowledge support from the National Science Foundation and Exxon Research and Engineering. We thank Prof. Hai Wang for providing us with the soot model.

References and Notes

(1) Santamaria, J.; Menendez, M.; Pena, J. A.; Barahona, J. L. *Catal. Today* **1992**, *13*, 353.
(2) Reyes, S. C.; Iglesia, E.; Kelkar C. P. *Chem. Eng. Sci.* **1993**, *48*, 2643.
(3) Reyes, S. C.; Kelkar, C. P.; Iglesia, E. *Catal. Lett.* **1993**, *19*, 167.
(4) Choudhary, V. R.; Choudhary, A. M.; Rajput, A. M.; Rane, V. H. *J. Chem. Soc.—Chem. Commun.* **1989**, *20*, 1526.
(5) Smith, K. J.; Painter, T. M.; Galuszka, J. *Catal. Lett.* **1991**, *11*, 301.
(6) Olsvik, O.; Rokstad, O. A.; Holmen, A. *Chem. Eng. Technol.* **1995**, *18*, 349.
(7) Rojnuckarin, A.; Floudas, C. A.; Rabitz, H.; Yetter, R. *Ind. Eng. Chem. Res.* **1996**, *35*, 683.
(8) Faliks, A.; Hall, R.; Floudas, C. A.; Rabitz, H.; Yetter, R. Submitted to *Ind. Eng. Chem. Res.*
(9) Frenklach, M.; Wang, H. *23rd Symp. (Int.) Combust. [Proc.]* **1990,** 1559−1566.
(10) Shanno, D. F.; Phua, K. H. Minimization of unconstrained multivariable functions. *ACM Trans. Math. Software* **1980**, *6*, 618.
(11) Kee, R. J.; Rupley, F. M.; Miller. J. A. *CHEMKIN-II: A Fortran Chemical Kinetics Package*, Sandia National Laboratories, 1989.
(12) Hindmarsh, A. C. *Odepack, A Systemized Collection of Ode Solvers in Scientific Computing;* North-Holland: Amsterdam, 1983.
(13) Kramer, M. A.; Calo, J. M.; Rabitz, H. *Appl. Math. Model* **1981**, *5*, 432.
(14) Frenklach, M.; Gardiner, Jr., W. C. *J. Phys. Chem.* **1984**, *88*, 6263.
(15) Frenklach, M. *Chem. Eng. Sci.* **1985**, *40*, 1843.
(16) Neoh, K. G.; Howard, J. B.; Sarofim, A. F. In *Pariculate Carbon: Formation During Combustion;* Siegla, D. C., Smith, G. W., Eds.; Plenum: New York, 1981.
(17) Glassman, I.; Nishida, O.; Sidebotham, G. In *Soot Formation in Combustion*; Toennis, P., Ed.; Springer-Verlag: New York, 1994; pp 316−324.